Plasma Flow Simulation of an MPD Thruster with an Electrode Model

IEPC-2015-201ISTS-2015-b-201

Presented at Joint Conference of 30th International Symposium on Space Technology and Science
34th International Electric Propulsion Conference and 6th Nano-satellite Symposium,
Hyogo-Kobe, Japan
July 4 – 10, 2015

Akira Kawasaki[1]
Tokyo Institute of Technology, Yokohama, Kanagawa, 226-8503, Japan

Kenichi Kubota[2]
Japan Aerospace Exploration Agency, Chofu, Tokyo, 182-8522, Japan

Ikkoh Funaki[3]
Japan Aerospace Exploration Agency, Sagamihara, Kanagawa, 252-5210, Japan

and

Yoshihiro Okuno[4]
Tokyo Institute of Technology, Yokohama, Kanagawa, 226-8503, Japan

Abstract: Plasma flow in a 100-kWe-class, steady-state, self-field magnetoplasma-dynamic (MPD) thruster was coupled with an electrode model and numerically simulated including electrode sheath. By the coupling with the electrode model, distributions of current density, sheath voltage, and wall heat flux were evaluated quantitatively on electrode based on a prescribed distribution of electrode temperature. It was shown that, within the cathode sheath, the principal carrier of electric charge is electron and discharge current density tends to be high in the region where cathode temperature is relatively high. The contribution of cathode sheath voltage to the discharge voltage was non-negligible. Wall heat flux on the cathode was mainly determined by the fluxes of emitted electrons from the cathode, absorbed plasma electrons to the cathode, and ions while neutral atoms did not significantly affect the heat flux.

Nomenclature

B	=	magnetic flux density
$\boldsymbol{B}$	=	magnetic flux density vector
D	=	diffusion coefficient
E	=	energy density, electric field
e	=	elementary charge
$\boldsymbol{e}$	=	unit vector
F_{EM}	=	electromagnetic thrust
$\bar{I}$	=	unit tensor

[1] Doctoral Student, Department of Energy Sciences, kawaswaki.a.ac@m.titech.ac.jp.
[2] Researcher, Aeronautical Technology Directorate.
[3] Associate Professor, Institute of Space and Astronautical Science.
[4] Professor, Department of Energy Sciences.

J_d = discharge current
j = current density
$\boldsymbol{j}$ = current density vector
k = Boltzmann constant
$\dot{m}$ = propellant mass flow rate
n = number density
p = (static) pressure
q = heat flux
r = radius, radial coordinate
s = length parameter along wall
T = temperature
t = time
U = internal energy density, diffusion velocity
$\boldsymbol{U}$ = diffusion velocity vector
u = velocity
$\boldsymbol{u}$ = velocity vector
V = voltage
x = distance from wall
Y = mass fraction
z = axial coordinate
α = electrode coefficient
β = Hall parameter
Γ = particle flux
δE = energy relaxation from electron to heavy particle
λ = thermal conductivity
μ_0 = space permeability
ρ = mass density
σ = electrical conductivity
$\bar{\boldsymbol{\tau}}$ = viscous stress tensor
ϕ = work function

Superscripts
ab : absorbed to wall
em : emitted from wall

Subscripts
a : anode
ave : average
B : Bohm
b : bulk plasma
c : cathode
e : electron
eff : effective
h : heavy species
i : ion
n : neutral atom, direction normal to wall surface
s : species
SE : sheath edge (boundary between sheath and bulk plasma)
sh : sheath
surf : surface
t : direction tangential to wall surface
tot : total
z : z component

I. Introduction

MAGNETOPLASMADYNAMIC (MPD) thruster is a type of electric propulsion device for space flights and it is driven by arc discharge[1]. Although there are some categories as for MPD thruster, steady-state, self-field MPD thrusters (hereafter, simply referred as "MPD thrusters") are particularly expected as one of prospective candidates of the next generation's high-power electric propulsion device for large scale space missions, e.g. exploration of the Moon, Mars, or Jupiter icy moons because the MPD thrusters can process large electric powers at light thruster weights and thus can exert preferable thrust-to-weight ratios.

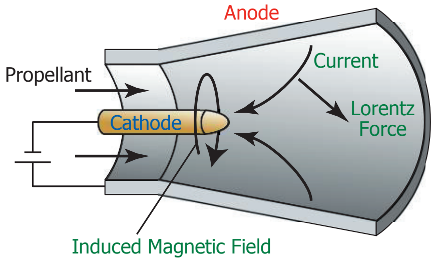

Figure 1. Operation concept of MPD thruster.

Figure 1 shows the operation concept of an MPD thruster. To generate thrust, the MPD thruster ionizes a propellant and accelerates it gas-dynamically and electromagnetically by high-intensity arc discharge (typically > 1 kA). Thus, the thrust of the MPD thruster is to consist of two components: gas-dynamic thrust, which is attributed to the Joule heating by the discharge current, and electromagnetic thrust, which is attributed to the Lorentz force as the interaction between the discharge current and the magnetic field induced by the current.

It is well known that, for efficient operation of the MPD thruster, contribution of the electromagnetic thrust needs to be significant enough. The discharge current, therefore, has to be adequately intensive. The high-intensity arc discharge, however, can lead to a large potential fall in the vicinity of the cathode, which often accounts for several dozen percent of the total discharge voltage[2]. The high-intensity arc discharge can also lead to severe heat load to the electrode. Hence, for precise prediction of the thruster state by numerical simulation, special consideration for the cathode sheath is to be required.

Until now, for MPD thrusters, some authors have conducted plasma flow simulations including the cathode sheath by incorporating electrode models[3,4]. However, there still remains room to improve the simulation models because some important realistic effects (such as thermionic emission and spatial variation of sheath) have not necessarily been considered. Kubota *et al.*[5], therefore, have extended the electrode model by Fujita and Arakawa[6] for weakly ionized plasma in a DC arcjet and performed plasma flow simulation coupled with the electrode model. Note that, in the simulation, cathode temperature distribution was determined depend on evaluated sheath fall voltage distribution.

In the present paper, an electrode model, in which thermionic emission and spatial variation of cathode sheath are considered, is coupled with a plasma flow model and plasma flow simulation is performed for a 100-kWe-class, steady-state, self-field MPD thruster (ZT3-IRS[7,8]) based on an experimentally measured temperature distribution of the cathode[9].

II. Numerical Model and Procedure

In the present paper, plasma flow and electrode sheath are separated and treated by distinguished models. The plasma flow is simulated based on a magnetohydrodynamic (MHD) flow model. The sheath is considered only in the vicinity of the cathode.

A. Plasma Flow Model

Steady-state argon plasma flow in the thruster is numerically simulated based on the following two-dimensional, axisymmetric, MHD fluid model[10,11]. In the simulation, the MHD equations and the generalized Ohm's law are solved with real gas effects: thermal non-equilibrium between heavy species (neutral atom and monovalent ion) and electron, chemical non-equilibrium for ionization, the Hall effect, electron pressure diffusion, diffusion, viscosity, thermal conduction, and compressibility. The equations are discretized by the finite volume method. The convection terms and the diffusion terms are evaluated by the 2nd-order TVD Lax-Friedrichs scheme[12] and the 2nd-order central difference respectively. Steady-state solutions are obtained by time marching with the explicit Euler method. Noted that good agreement between the results in numerical simulation and experiment has been confirmed for a certain thruster[10].

The basic equations are as follows: the equation of total mass

$$\frac{\partial \rho}{\partial t} + \nabla \cdot (\rho \boldsymbol{u}) = 0 \tag{1}$$

the equation of ion mass

$$\frac{\partial \rho Y_s}{\partial t} + \nabla \cdot (\rho Y_s \boldsymbol{u}) = -\nabla(\rho D_s \nabla Y_s) + \rho \dot{Y}_s \qquad (s = \mathrm{Ar}^+) \tag{2}$$

the equation of momentum

$$\frac{\partial \rho \boldsymbol{u}}{\partial t} + \nabla \cdot (\rho \boldsymbol{u}\boldsymbol{u} + p\bar{\boldsymbol{I}}) = \nabla \cdot \bar{\tau} + \boldsymbol{j} \times \boldsymbol{B} \tag{3}$$

the equation of heavy particle total energy

$$\frac{\partial E_h}{\partial t} + \nabla \cdot [(E_h + p)\boldsymbol{u}] = p_e \nabla \cdot \boldsymbol{u} + \nabla \cdot (\bar{\boldsymbol{\tau}}\boldsymbol{u}) + \nabla \cdot (\lambda_h \nabla T_h) + \boldsymbol{u} \cdot (\boldsymbol{j} \times \boldsymbol{B}) + \delta E \tag{4}$$

the equation of electron internal energy

$$\frac{\partial U_e}{\partial t} + \nabla \cdot (U_e \boldsymbol{u}) = -p_e \nabla \cdot \boldsymbol{u} + \nabla \cdot \left(\lambda_e \nabla T_e + \frac{5}{2} \frac{kT_e}{e} \boldsymbol{j} \right) + \frac{\boldsymbol{j}^2}{\sigma} - \frac{1}{en_e} \boldsymbol{j} \cdot \nabla p_e - \delta E - \dot{n}_i V_i \tag{5}$$

and the induction equation

$$\frac{\partial \boldsymbol{B}}{\partial t} - \nabla \times (\boldsymbol{u} \times \boldsymbol{B}) = -\nabla \times \frac{1}{\mu_0 \sigma} \left[\nabla \times \boldsymbol{B} + \beta_e (\nabla \times \boldsymbol{B}) \times \frac{\boldsymbol{B}}{B} - \mu_0 \beta_e \nabla p_e \right] \tag{6}$$

where, the energy densities in the above mentioned equations are defined as follows

$$E_h = \frac{3}{2} n_h k_B T_h + \frac{1}{2} \rho \boldsymbol{u}^2 \tag{7}$$

$$U_e = \frac{3}{2} n_e k_B T_e \tag{8}$$

For the current density and the pressures, the following relations are assumed: Ampère's law

$$\boldsymbol{j} = \frac{1}{\mu_0} \nabla \times \boldsymbol{B} \tag{9}$$

and the equation of state of ideal gases

$$p = \sum_s p_s + p_e, \quad p_s = n_s k_B T_h, \quad p_e = n_e k_B T_e \quad (s = \mathrm{Ar}, \mathrm{Ar}^+) \tag{10}$$

B. Electrode Model

In the present paper, an electrically non-neutral space-charge layer formed in the vicinity of a wall is referred to as a sheath. In general, sheaths of bounded plasmas are very thin and they have thicknesses of the order of the Debye length. Moreover, within the sheaths, the charge neutrality is not satisfied. Thus, the plasma flow model cannot resolve the sheath region. Hence, in the present paper, an electrode model (EM) based on a model by Prewett and Allen[13] is adopted as a boundary condition of the plasma flow simulation.

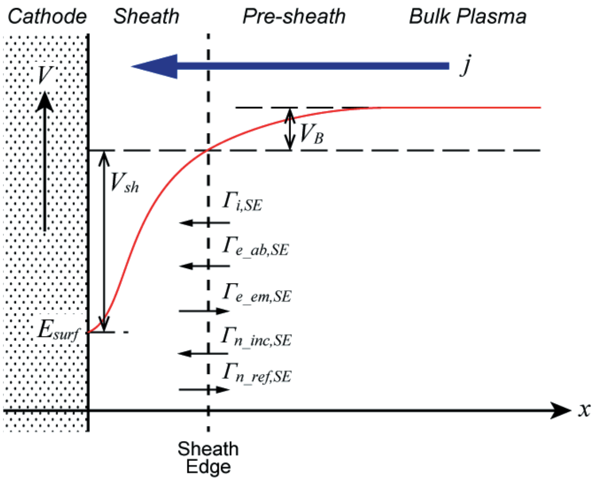

Figure 2. Conceptual scheme of cathode sheath.

The conceptual scheme of the cathode sheath in this model is shown in Figure 2. The x-coordinate is set from the cathode. It is assumed that an ion-rich (electron repelling) sheath is formed in front of the cathode. In this model, cathode sheath voltage (potential at the sheath edge relative to the cathode), and electric field intensity on the cathode surface are determined by solving the following equations: the matching equation of current density at the sheath edge

$$j_{tot} = j_{i,SE} + j_{e,SE}^{ab} + j_{e,SE}^{em} \tag{11}$$

and the matching equation of electric field intensity on the cathode

$$\varepsilon^2 = 4\nu_i \eta_B \left[\sqrt{1 + \frac{\eta_{sh}}{\eta_B}} - 1 \right] - 4J_b \left[\sqrt{\eta_{sh} + E_b} - \sqrt{E_b} \right] + 2\exp(-\eta_{sh}) - 2 \tag{12}$$

The current densities are defined as follows

$$j_{tot} = \frac{1}{\mu_0} \nabla \times \boldsymbol{B} \tag{13}$$

$$j_{i,SE} = e\Gamma_{i,SE} = -en_{i,SE} u_B, \quad n_{i,SE} = n_{e,SE}^{ab} + n_{e,SE}^{em} \tag{14}$$

$$j_{e,SE}^{ab} = -e\Gamma_{e,SE}^{ab} = \frac{1}{4} en_{e,SE}^{ab} \overline{C}_{e,SE} \exp\left(-\frac{eV_{sh}}{kT_{e,SE}} \right) \tag{15}$$

$$j_{e,SE}^{em} = -e\Gamma_{e,SE}^{em} = -AT_c^2 \exp\left(-\frac{e\phi_{eff}}{kT_c} \right), \quad \phi_{eff} = \phi - \sqrt{\frac{eE_{surf}}{4\pi\varepsilon_0}} \tag{16}$$

The quantities within Equation (12) are defined as follows

$$\varepsilon = \frac{e\lambda_D E_{surf}}{k_B T_e}, \quad \eta_B = \frac{eV_B}{kT_e} = \frac{\frac{1}{2} m_i u_B^2}{kT_e} = \frac{\nu_i}{2 - J_b (\eta_c + E_b)^{-3/2}},$$

$$\nu_i = \frac{n_{i,SE}}{n_{e,SE}} = 1 + \frac{J_b}{\sqrt{\eta_{sh} + E_b}}, \quad J_b = \frac{j_b}{en_{e,SE}}\sqrt{\frac{m_e}{2kT_e}}, \quad \eta_{sh} = \frac{eV_{sh}}{kT_e}, \quad E_b = \frac{2kT_c}{kT_e} \tag{17}$$

The following constraint relation is to be satisfied.

$$n^{em}_{e,SE} = \frac{j^{em}_{e,SE}}{e}\left(\frac{4kT_c}{m_e} + \frac{2eV_{sh}}{m_e}\right)^{-1} \tag{18}$$

Equations (11) and (12) are numerically solved with regard to V_{sh} and E_{surf} based on the input parameters of discharge current density, properties of ambient plasma (heavy species temperature, electron temperature, pressure, and ionization degree), and cathode temperature. The discharge current density and the properties of the ambient plasma are given by the plasma flow model.

Based on the determined particle fluxes, heat fluxes at the sheath edge can be evaluated as follows

$$q_{i,SE} = \left(2kT_{h,SE} + eV_B\right)\Gamma_{i,SE} \tag{19}$$

$$q^{ab}_{e,SE} = \left(2kT_{e,SE} + eV_{sh}\right)\Gamma^{ab}_{e,SE} \tag{20}$$

$$q^{em}_{e,SE} = \left(2kT_c + eV_{sh}\right)\Gamma^{em}_{e,SE} \tag{21}$$

$$q^{inc}_{n,SE} = 2kT_{h,SE}\Gamma^{inc}_{n,SE}, \quad \Gamma^{inc}_{n,SE} = -\frac{1}{4}n_{n,SE}\overline{C}_{h,SE} \tag{22}$$

$$q^{ref}_{n,SE} = 2kT_c\Gamma^{ref}_{n,SE}, \quad \Gamma^{refc}_{n,SE} = -\left(\Gamma_{i,SE} + \Gamma^{inc}_{n,SE}\right) \tag{23}$$

Wall heat fluxes are also evaluated as follows[14]

$$q_w = q_{i,w} + q^{ab}_{e,w} + q^{em}_{e,w} + q^{inc}_{n,w} + q^{ref}_{n,w} \tag{24}$$

$$q_{i,w} = -\left(2kT_{h,SE} + eV_B + eV_{sh} + e\phi_{ion} - e\phi_{eff}\right)\Gamma_{i,PB} \tag{25}$$

$$q^{ab}_{e,SE} = -\left(2kT_{e,SE} + e\phi_{eff}\right)\Gamma^{ab}_{e,SE} \tag{26}$$

$$q^{em}_{e,SE} = -\left(2kT_c + e\phi_{eff}\right)\Gamma^{em}_{e,SE} \tag{27}$$

$$q^{inc}_{n,SE} = -2kT_{h,SE}\Gamma^{inc}_{n,SE} \tag{28}$$

$$q^{ref}_{n,SE} = -2kT_c\Gamma^{ref}_{n,SE} \tag{29}$$

Here, basic characteristics of the electrode model are preliminarily investigated for the conditions tabulated in Table 1. For local analyses of the cathode sheath, typical conditions near the cathode are chosen for the benchmark case and cathode temperature is varied within a range where the thermionic emission is effective. As shown in Figure 3 (a), in general, cathode sheath voltage decreases with the increase in cathode wall temperature. This is because, in the present model, the sheath voltage is determined to match the sum of currents by charged particles within the sheath with discharge current density. Namely, as shown in Figure 3 (b), in the case where cathode temperature is high, because thermionic current is excessive to the discharge current and has to be canceled by back current by plasma electrons absorbed by the cathode, low sheath voltage is to be required. On the other hand, in the case where cathode temperature is low, because thermionic current has to be enhanced by the Schottky effect and the back current by the plasma electron has to be suppressed, high sheath voltage is to be required. As shown in Figure 3 (c), in the region of cathode temperature where thermionic current matches with discharge current, wall heat flux on the cathode is almost constant and in the order of 10^7 W/m^2. However, in the case where cathode temperature is excessively low, wall heat flux is large because of ions strongly accelerated by large cathode sheath voltage. In the case where cathode temperature is excessively high, wall heat flux is also large attributed that ambient electron temperature is higher than cathode temperature and that back current by plasma electrons is enhanced by low sheath voltage. As shown in Figure 3 (d), in the present model, the direction of heat flux at the sheath edge can be altered depend on conditions. That is, in the case where cathode temperature is relatively low, heat flows toward the bulk plasma, and in the case where cathode temperature is relatively high, the situation is opposite.

Table 1. Conditions for local analysis of electrode model.

Item	Condition
Ambient gas	Ar
Discharge current density, A/m^2	-2.0 x 10^6
Ambient heavy species temperature, K	1000
Ambient electron temperature, K	1500
Ambient pressure, Pa	2000
Ambient ionization degree	0.2
Cathode temperature, K	2200 - 3200
Cathode material	W-ThO_2

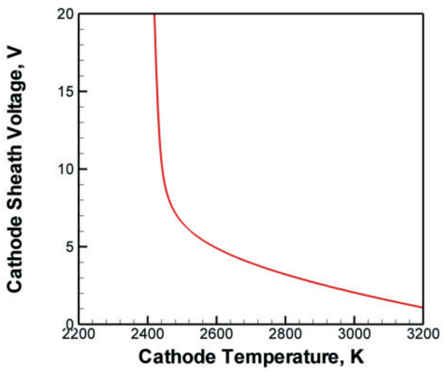

(a) Cathode sheath voltage.

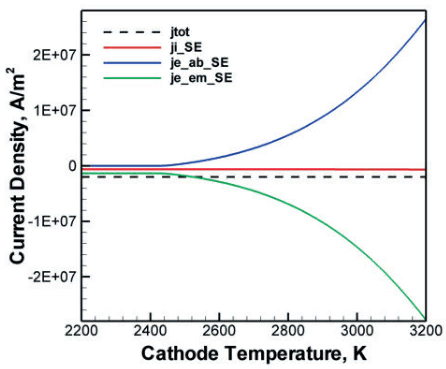

(b) Composition of current within cathode sheath.

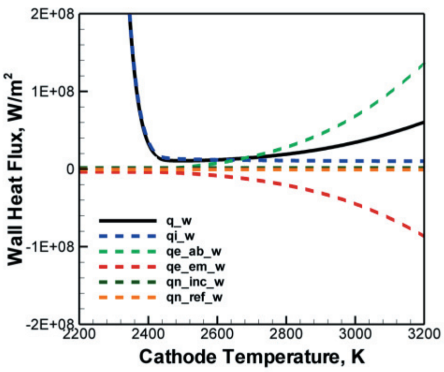

(c) Wall heat flux and components.

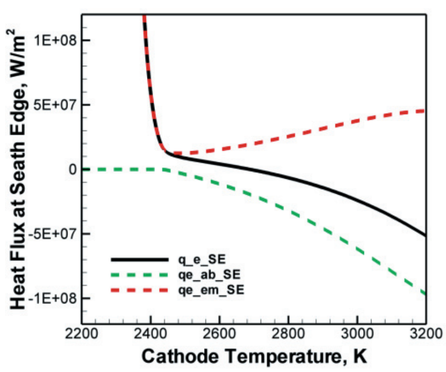

(d) Heat flux at sheath edge and components.

Figure 3. Physical quantities on cathode as functions of cathode temperature.

C. Simulation Conditions

Simulation conditions are tabulated in Table 2. For velocity, the non-slip condition is imposed on the walls. Boundary temperature of heavy particles is set to the same value as the electrodes, where anode temperature is set to 300 K and cathode temperature is set to temperature measured by the Institute of Space System (IRS) of the University of Stuttgart[9], which is shown in Figure 3. Boundary temperature of electron is set to below 300 K (limited isothermal condition). The azimuthal magnetic flux density at the inlet is determined by the Ampère's law.

$$B_\theta = -\frac{\mu_0 J_d}{2\pi r_c} \tag{30}$$

The existence of the cathode sheath influences the boundary condition of azimuthal induced magnetic field. Since the boundaries of the computational domain correspond to sheath edge, a relevant boundary condition should be

$$E_t = -\frac{dV_{sh}}{ds} \tag{31}$$

In Equation (31), E_t can be represented as the function of azimuthal induced magnetic field with the aid of the generalized Ohm's law and the Ampère's law. A nonlinear equation with regard to the induced magnetic field is numerically solved on the electrodes.

Table 2. Simulation conditions.

Item	Condition
Propellant	Ar
Mass flow rate, g/s	2
Discharge current, kA	10
Inlet heavy particle temperature, K	300
Inlet electron temperature, K	300
Inlet ionization degree	1×10^{-5}
Anode temperature, K	300
Cathode temperature, K	given in Figure 4
Electron temperature on wall, K	300
Electrode material	$W\text{-}ThO_2$

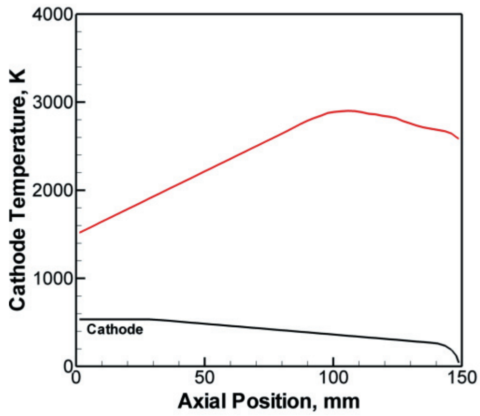

Figure 4. Cathode temperature distribution[9].

Computation grid is shown in Figure 5. In the present paper, thruster configuration is conformed to ZT3-IRS thruster[7,8]. Simulation has been performed for the six cases tabulated in Table 3. In Case A, plasma flow simulation is performed without the electrode model while plasma flow is coupled with the electrode model and simulated in Case B.

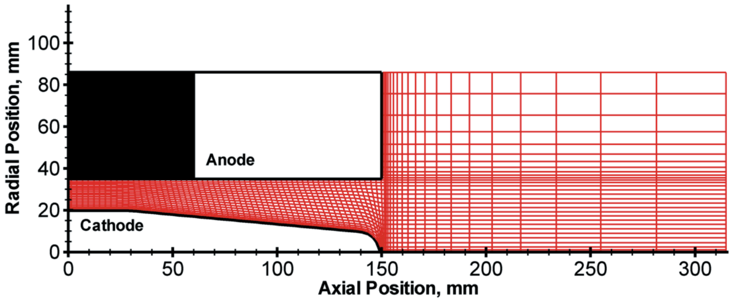

Figure 5. Computation grid.

Table 3. Simulation cases.

Case	EM	J_d	T_c
A		-	-
B	✓	-	-
B_{Jd-}	✓	-5%	-
B_{Jd+}	✓	+5%	-
B_{Tc-}	✓	-	-5%
B_{Tc+}	✓	-	+5%

III. Results and Discussion

D. Influence of Coupling with the Electrode Model

In Figure 6, distributions of physical quantities on the cathode are shown. The distributions of sheath voltage and current density on the cathode are determined by interactions among them and properties of plasma under certain temperature distribution of cathode, which is show in Figure 6 (a). As shown in Figure 6 (b), cathode sheath voltage is relatively low in the regions where cathode temperature is relatively high (z ~ 90 – 130 mm) and current density is relatively low (z ~ 0 -20, 150 mm). In Figure 6 (c), current density distributions in Case A and B are shown by the dashed line and the solid line respectively. In Case B where the electrode model is coupled, compared with the distribution in Case A where the electrode model is not coupled, current is sifted toward the point where cathode temperature is maximum (z ~ 100 mm). This result indicates that distribution of intensity of thermionic electric emission, which is mainly depend on temperature, is reflected on the current distribution by coupling with the electrode model. However, it should be noted that current distribution is not simply similar to cathode temperature distribution. This is because intensity of thermionic electron emission is affected not only by cathode temperature but also by the Schottky electric field. It is also thought to be one of the reasons that current distribution can be affected by the Hall effect. In Figure 6 (d), estimated wall heat flux distribution on the cathode is shown. The distribution of heat flux is roughly similar to the distribution of current density. Namely, heat flux is relatively high in the region where current density is relatively high (z ~ 70 – 150 mm). The value of heat flux is in the order of 10^6 to 10^7 W/m^2 and it is consistent with experimentally measured value[15].

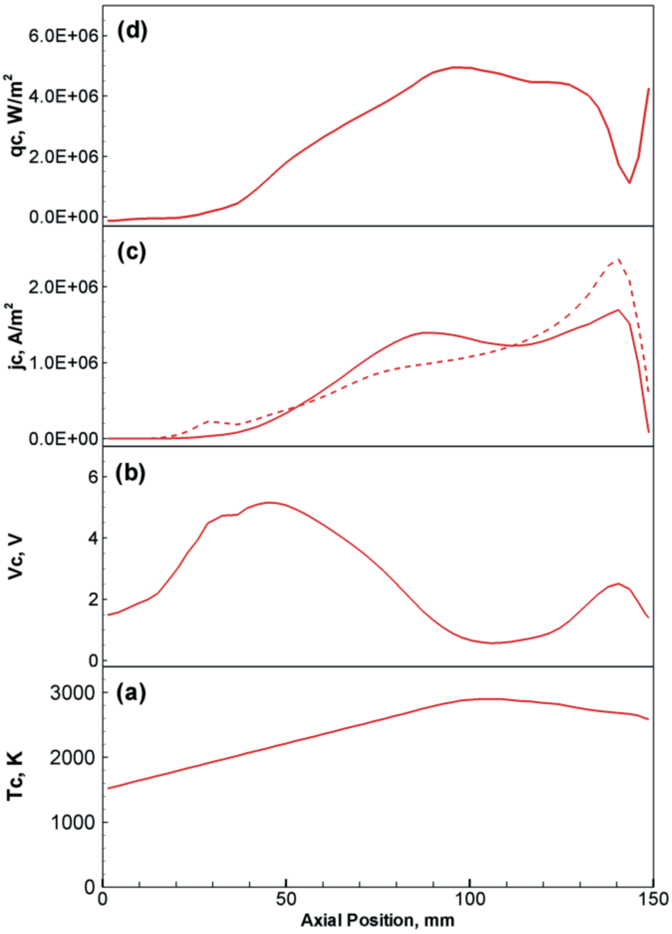

Figure 6. Distributions of (a) cathode temperature, (b) cathode sheath voltage, (c) current density on cathode and (d) wall heath flux on cathode. Dashed line in (c) represent the result in Case A. (Case B, Ar, 2.0 g/s, 10 kA)

Distribution of current density on cathode and its components in cathode sheath are shown in Figure 7. In the model of the present paper, local discharge current density is determined as net quantity by balance among fluxes of ion, absorbed electron, and emitted electron. In the region where cathode temperature is relatively high (z ~ 50 -150 mm), absorbed and emitted electron are major carriers of electric charge within sheath. Additionally, in the region where cathode temperature is relatively high, thermionic current is excessive compared to discharge current density and is canceled by large back current by plasma electron. Emitted electron current (thermionic current) density and absorbed electron current (back current by plasma electron) density have maxima in the vicinity of the point where cathode temperature is maximal (z ~ 100 mm).

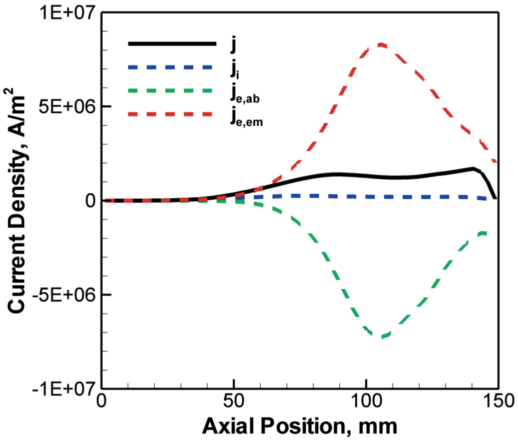

Figure 7. Distribution of current density on cathode and its components in cathode sheath. (Case B, Ar, 2.0 g/s, 10 kA)

Distribution of wall heat flux on cathode and its components are shown in Figure 8. In association with that electron is major carrier of electric charge within sheath, contribution of absorbed and emitted electron to wall heat flux on cathode is also most dominant. In the region where cathode temperature is particularly high (z ~ 70 – 150 mm), heat fluxes by excessive thermionic electron and plasma electron, which cancels thermionic electron, are roughly ten times as large as net wall heat flux. With regard to contribution of ion, although it is not major carrier of electric charge, heat flux by ion is comparable with net wall heat flux. This is due to that ions are accelerated in the sheath, and that the ions recombine on cathode surface and gives ionization energy to the wall. Note that, in the present model, ions are assumed to recombine on wall with probability 1. With regard to neutral atom, contribution to wall heat flux is relatively insignificant.

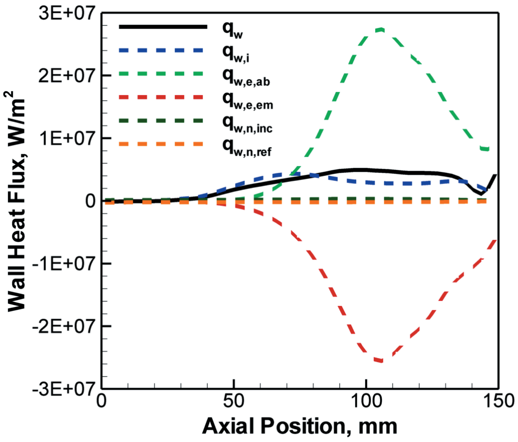

Figure 8. Distribution of wall heat flux on cathode and its components. (Case B, Ar, 2.0 g/s, 10 kA)

Comparison of current lines and flow field between Case A and B is shown in Figure 9. In Case B, the current lines near the cathode are shifted toward the position where cathode temperature is maximum as described above. Nevertheless, no significant change is seen in the vicinity of anode. Therefore, no significant change is seen in the flow field.

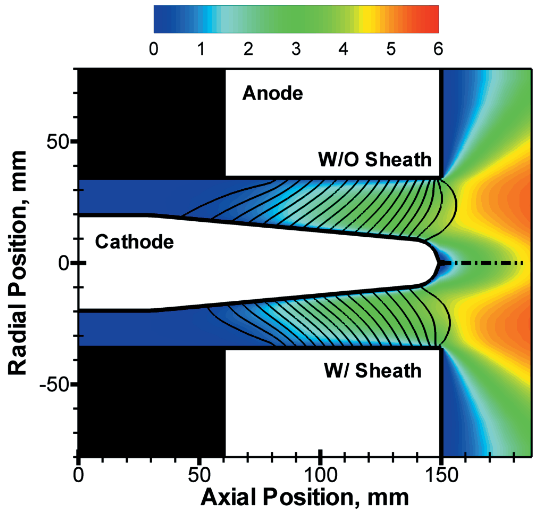

Figure 9. Comparison of current lines (black lines) and axial velocity (km/s) distribution (color map) in the thruster. The upper half corresponds to the result in Case A and the lower half the result in Case B. (Ar, 2.0 g/s, 10 kA)

In Table 4, comparison of thruster characteristics between Case A and B are presented. In the present paper, thrusts and their components are evaluated by the following equations,

$$F = F_{GD} + F_{EM} \tag{32}$$

$$F_{GD} = \iint_{\text{Inlet}} \left[p + \rho(\boldsymbol{u}\cdot\boldsymbol{e}_z)^2 - \boldsymbol{e}_n\cdot\bar{\boldsymbol{\tau}}\cdot\boldsymbol{e}_z\right]\boldsymbol{e}_z\cdot d\boldsymbol{S} + \iint_{\text{Anode-side wall}} (p - \boldsymbol{e}_n\cdot\bar{\boldsymbol{\tau}}\cdot\boldsymbol{e}_z)\boldsymbol{e}_z\cdot d\boldsymbol{S} \tag{33}$$

$$F_{EM} = \iiint [(\boldsymbol{j}\times\boldsymbol{B})\cdot\boldsymbol{e}_z]dV + \iint_{\text{Cathode-side wall}} (p - \boldsymbol{e}_n\cdot\bar{\boldsymbol{\tau}}\cdot\boldsymbol{e}_z)\boldsymbol{e}_z\cdot d\boldsymbol{S} \tag{34}$$

discharge voltages and their components are evaluated by the following equations,

$$V_d = V_{a,ave} + V_{b,ave} + V_{c,ave} \tag{35}$$

$$V_{a,ave} = \iint_{\text{Aathode}} \boldsymbol{j}V_a\cdot d\boldsymbol{S} \Big/ J_d \tag{36}$$

$$V_{b,ave} = \iiint_{\text{Bulk plasma}} (\boldsymbol{j}\cdot\boldsymbol{E})dV \Big/ J_d \tag{37}$$

$$V_{c,ave} = \iint_{\text{Cathode}} \boldsymbol{j}V_c\cdot d\boldsymbol{S} \Big/ J_d \tag{38}$$

Between Case A and B, there is no significant difference with regard to the evaluated thrust although electromagnetic thrust is slightly changed because of the change in current lines on the cathode. On the other hand, apparent difference is seen with regard to the evaluated discharge voltage by cathode fall voltage. The difference is ca. 22% and thus the contribution of cathode sheath voltage is to be non-negligible for performance evaluation.

Table 4. Comparison of typical thruster characteristics between Case A and B. (Ar, 2.0 g/s, 10 kA)

Item	Case A	Case B
Thrust, N	10.6	10.5
- Gas-dynamic thrust, N	2.0	2.3
- Electromagnetic thrust, N	8.6	8.2
	(81%)	(78%)
Discharge voltage, V	9.9	12.1
- Bulk plasma, V	9.9	10.0
- Cathode sheath, V	0.0	2.1
		(17%)

E. Dependence on Simulation Conditions

Typical thruster characteristics for Case B, B_{Jd-}, B_{Jd+}, B_{Tc-}, and B_{Tc+} are tabulated in Table 5. Thrust is increased with the increase in discharge current but decreased with the increase in cathode temperature. The reason why thrust is decreased with the increase in cathode temperature is to be attributed to shift of current on cathode toward the root as is described below. Discharge voltage is increased with the increase in discharge current but decreased with the increase in cathode temperature. The contribution of the cathode sheath voltage to the discharge voltage is increased with the increase in discharge current. This is thought to be due to that cathode temperature distribution is fixed. The contribution of the cathode sheath voltage to the discharge voltage is decreased with the increase in the cathode temperature. This is thought to be due to that discharge current is fixed.

Relative changes in thrust, discharge voltage, and cathode sheath voltage to Case B are shown in Figure 10. With regard to the thrust and discharge voltage, the relative changes to ±5% changes in discharge current and cathode temperature is within ±10%. Relative change in cathode sheath voltage is also within ±10% to ±5% changes in discharge current. On the other hand, relative change in cathode sheath voltage is several dozen percent to ±5% changes in cathode temperature. In short, cathode sheath is sensitive to a change in cathode temperature. Therefore, for a precise numerical simulation, validity of the assumption of cathode temperature is very important. In the present paper, the assumption of the cathode temperature is based on the result of the experimental measurement. When simulations are performed for arbitrary thrusters, thermal analysis of cathode temperature is need to be coupled.

Table 5. Comparison of typical thruster characteristics among Case B's. (Ar, 2.0 g/s, 10 kA)

Item	Case B	Case B_{Jd-}	Case B_{Jd+}	Case B_{Tc-}	Case B_{Tc+}
Thrust, N	10.5	10.0	11.2	11.0	10.4
Discharge voltage, V	12.1	11.6	12.8	12.9	12.1
- Bulk plasma, V	10.0	10.7	10.5	9.2	10.8
- Cathode sheath, V	2.1	1.9	2.3	3.7	1.3
	(17%)	(16%)	(18%)	(29%)	(11%)

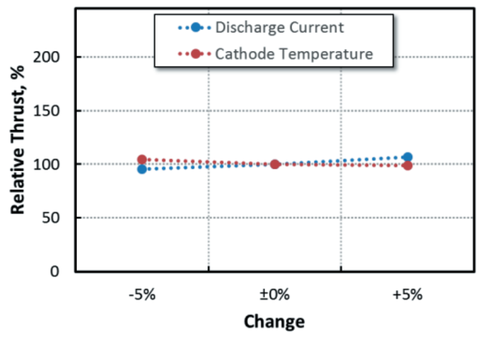

(a) Relative thrust.

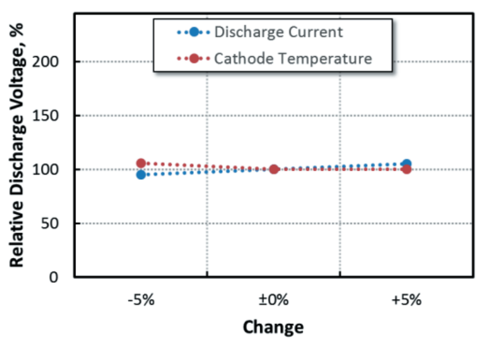

(b) Relative discharge voltage.

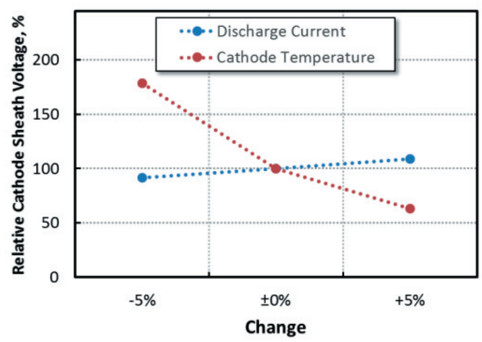

(c) Relative cathode sheath voltage.

Figure 10. Relative change to Case B (baseline). (Ar, 2.0 g/s, 10 kA)

The dependences of the discharge current density distribution on cathode on the discharge current and the cathode temperature are shown in Figure 11. Discharge current density is increased with the increase in discharge current almost similarly. On the other hand, discharge current distribution is shifted toward the cathode root by the increase in cathode temperature.

The dependences of the cathode sheath voltage distribution on the discharge current and the cathode temperature are shown in Figure 12. Cathode sheath voltage is increased with the increase in the discharge current almost similarly, but the increase in the cathode sheath voltage in the region where the cathode temperature is particularly high ($z \sim 70 - 130$ mm) is relatively insignificant. This is because, in the region where the cathode temperature is high, the influence of the increase in current density is insignificant to intensive thermionic current density. Cathode sheath voltage is decreased with the increase in the cathode temperature almost similarly. In particular, near the cathode tip ($z \sim 100 - 150$ mm), change is significant. This is thought to be related to the shift of the discharge current distribution on the cathode as described above.

The dependence of the wall heat flux on the cathode on the discharge current and the cathode temperature are shown in Figure 13. Wall heat flux is increased with the increase in the discharge current almost similarly. With the increase in the cathode temperature, the wall heat flux is shifted toward cathode root as it is for the discharge current density on the cathode.

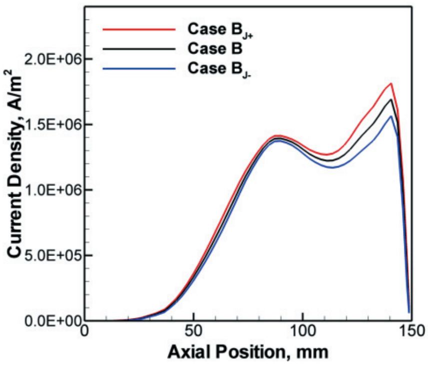

(a) Dependence on discharge current. **(b) Dependence on cathode temperature**

Figure 11. Discharge current density distribution on cathode. (Ar, 2.0 g/s, 10 kA)

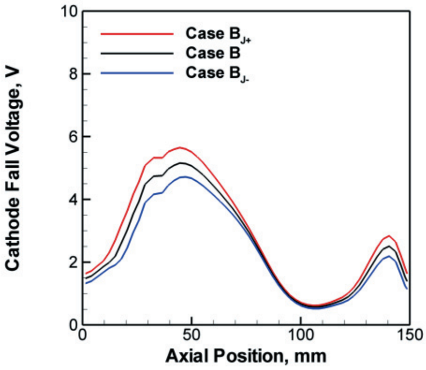

(a) Dependence on discharge current. **(b) Dependence on cathode temperature**

Figure 12. Cathode sheath voltage distribution. (Ar, 2.0 g/s, 10 kA)

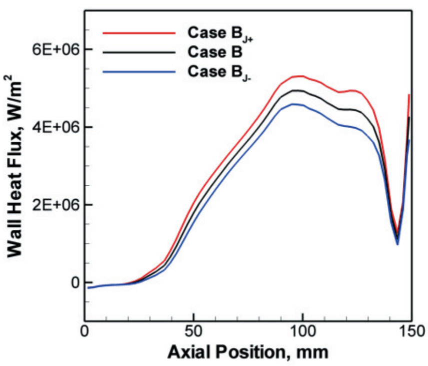

(a) Dependence on discharge current. **(b) Dependence on cathode temperature**

Figure 13. Wall heat flux distribution on cathode. (Ar, 2.0 g/s, 10 kA)

IV. Conclusions

Plasma flow in a 100-kWe-class, steady-state, self-field MPD thruster (ZT3/IRS) have been coupled with an electrode model and numerically simulated. As a result, the following conclusions have been drawn.

- By the coupling of the plasma flow model with the electrode model, distributions of the discharge current density on the cathode, the cathode fall voltage, and the wall heat flux on the cathode can be evaluated quantitatively based on conditions of the plasma flow and the cathode.
- Within the cathode sheath, major carrier of electric charge is electron. Although current density on the cathode tends to be high in the region where cathode temperature is relatively high, the distribution of the current density is not necessarily similar to the distribution of cathode temperature.
- The contribution of the cathode sheath voltage is significant for the discharge voltage.
- Wall heat flux on the cathode is mainly determined by emitted electrons from the cathode, absorbed electrons to the cathode, and ions. The influence of the neutral atoms is relatively insignificant for the wall heat flux.

Acknowledgments

This work was supported by JSPS KAKENHI Grant Number 15J10821.

References

[1]Jahn, R. G., *Physics of Electric Propulsion*, McGraw-Hill, New York, 1968.

[2]Nakata, D., "Experimental Measurement of Total Sheath Fall Voltage in an MPD Thruster," *44th AIAA/ASME/SAE/ASEE Joint Propulsion Conference & Exhibit*, AIAA Paper 2008-4635, Hartford, CT, USA, 2008.

[3]Boie, C., Kaeppeler, H. J., Sleziona, P. C., and Auweter-Kurtz, M., "Application of Adaptive Numerical Schemes for MPD Thruster Simulation," *25th International Electric Propulsion Conference*, IEPC-97-115, Cleveland, Ohio, USA, 1997.

[4]Roy, S., "Self Consistent Electrode Model for Magnetoplasmadynamic Thrusters," *40th AIAA/ASME/SAE/ASEE Joint Propulsion Conference*, AIAA Paper 2004-3469, Fort Lauderdale, Florida, USA, 2004.

[5]Kubota, K., Funaki, I., Okuno, Y., "Numerical Study on Electrode Model for Plasma Simulation of MPD Thruster," *32nd International Electric Propulsion Conference*, IEPC-2011-252, Wiesbaden, Germany, 2011.

[6]Fujita, K., and Arakawa, Y., "Performance Computation of a Low-Power Hydrogen Arcjet," *Journal of Propulsion and Power*, Vol. 15, No. 1, pp. 144-150, 1999.

[7]Winter, M., Boie, C., Auweter-Kurtz, M., and Kurtz, H. L., "Experimental and Numerical Investigation of Steady State MPD Thrusters", *2nd European Spacecraft Propulsion Conference*, ESA SP-398, Noordwijk, Netherland, 1997.

[8]Auweter-Kurtz, M., "Plasma Thruster Development Program at the IRS," *Acta Astronautica*, Vol. 32, No. 5, 1994, pp. 377-391.

[9]Winter, M. W., Auweter-Kurtz, M., Kurtz, H. L., and Sleziona, P. C., "Evaluation of Cathode Tmeperature Distribution in a Cylindrical MPD Thruster," *24th International Electric Propulsion Conference*, IEPC-95-109, Moscow, Russia, 1995.

[10]Kubota, K., Funaki, I., and Okuno, Y. "Comparison of Simulated Plasma Flow Field in a Two-Dimensional Magnetoplasmadynamic Thrsuter with Experimental Data," *IEEE Transactions on Plasma Science*, Vol. 37, No. 12, 2009, pp. 2390-2398.

[11]Kubota, K., Sato, H., Funaki, I. and Okuno, Y., "Magnetohydrodynamic simulation of MPD thruster," *Journal of the Japan Society for Aeronautical and Space Sciences* (in Japanese), Vol. 59, 2011, pp. 396-401.

[12]Tóth, G., and Odstčril, D. "Comparison of Some Flux Corrected Transport and Total Variation Diminishing Numerical Schemes for Hydrodynamic and Magnetohydrodynamic Problems," *Journal of Computational Physics*, Vol. 128, No. 1, 1996, pp. 82-100.

[13]Prewett, P., and Allen, J., "The Double Sheath Associated with a Hot Cathode," *Proceedings of Royal Society of London A*, Vol. 348, Issue 1655, 1976, pp. 435-446.

[14]Goodfellow, K. D., "Theoretical Investigation of Cathode Operation in High-Power Arcjets," *31st Join Propulsion Conference and Exhibit*, AIAA Paper 95-3061, San Diego, CA, USA, 1995.

[15]Hügel, H., and Krülle, G., "Phänomenologie und Energiebilanz von Lichtbogenkathoden bei niedrigen Drucken und Hohen Stromstärken," *Beiträge aus der Plasmaphysik* (in German), Vol. 9, No. 2, 1969, pp. 87-116.